Three-dimentional measurement of a stress field in a rectangular channel flow using a photoelastic method

K. Nakamine[1] ,*Y Yokoyama[1], M. Muto [2], Y Tagawa[1]

1: Dept. of Mech. Sys. Eng., Tokyo University of Agriculture and Technology, Japan
2: Dept. of Mech. Sys. Eng., Nagoya Institute of Technology, Japan
* Corresponding author: s212494@st.go.tuat.ac.jp, tagawayo@cc.tuat.ac.jp

Keywords: Photoelaticity, Three-dimentional fluid stress, Laminar flow, Rectangular channel, High-speed polarization camera

The hydrodynamic stress field of a steady laminar flow in a rectangular channel was experimentally measured by using a photoelastic method. For this purpose, following two issues for a mixed solution of photoelastic material, cellulose nanoctystal (CNC), were extensively investigated. The first is to elucidate whether there are any phenomena (trends) peculiar to a CNC-mixed solution that differ from those to the solid case. The second is to elucidate the extent to which the stress-optic law holds for CNC mixed solution. As a verification method for the first question, we measured retardation distributions by using a high-speed polarization camera. We compared distributions of measured retardation of a CNC mixed solution (0.5 wt %) (Newtonian fluid) and theoretical secondary-principal stress difference derived from the analytical solution of steady laminar flow in a rectangular channel. The results showed that a retardation, which was not affected by stress-oriented phase retardation, appeared in the CNC mixed solution. The reason is considered to be retardation induced by aggregations of CNC particles. This phenomenon is peculiar to CNC mixed solution and does not occur in solids cases. As a method of verification of the second issue, we compared the secondary principal stress difference distribution with the retardation distribution offsetting the effect of the retardation specific to the CNC mixed solution. The result showed that the spatial intensity distributions of both agreed within a relative error of 3.84 %. This indicates that the stress-optic law holds for the retardation offsetting the retardation specific to the CNC mixed solution. To evaluate the validity of the above validation results, we measured the retardation fields of flows at different flow rates (10, 20 ml/min). The measured results agree with theory with relative errors 5.67 % and 3.24 % for flow rates of 10 and 20 ml/min, respectively. These results indicate that the method presented here is promising for measuring three-dimensional stress field in a flow.

1. Introduction

To elucidate the mechanism of angiopathy such as cerebral aneurysms, the measurement of localized strong shear stress inside a cerebral vessel wall is crucial (Meng et al., 2007; Shojima et al., 2004). However, such stress measurement is challenging because of three-dimensional hydraulic stress distribution inside a small cerebral blood vessels and the unsteady flow field with pulsation.

Therefore, three-dimensional measurement method for hydraulic stress field is expected. Muto et al. visualized the unsteady fluid stress field using a photoelastic method (MUTO & TAGAWA, 2019). In this method, the retardation of the polarized light passing through photoelastic material under stress is measured by a high-speed polarization camera. Note that the retardation measured by the high-speed polarization camera is the integrated value along the optical axis of the camera. In a two-dimensional stress field with no stress component in the optical axis of the camera, the retardation Δ is proportional to the principal stress difference σ_d (Ramesh, 2021). The relationship is called the stress-optic law and described as

$$\Delta = Ch\sigma_d = Ch\left(\sigma_1 - \sigma_2\right) \tag{1}$$

where h [m] is the thickness of the measurement object in the optical axis of the camera, C [1/Pa] is the stress-optic coefficient, σ_d [Pa] is the principal stress difference, σ_1, σ_2 [Pa] are respectively the maximum and minimum principal stress (see Fig. 1). In Eq. (1), in a two-dimensional stress field where the stress distribution in xy-plane is constant at any z, the retardation is proportional to the principal stress difference because the value of the principal stress difference is constant in z direction. On the other hand, in a three-dimensional stress field where the stress distribution in xy-plane varies with z, the relation between the hydraulic stress field and the integrated retardation should be examined carefully.

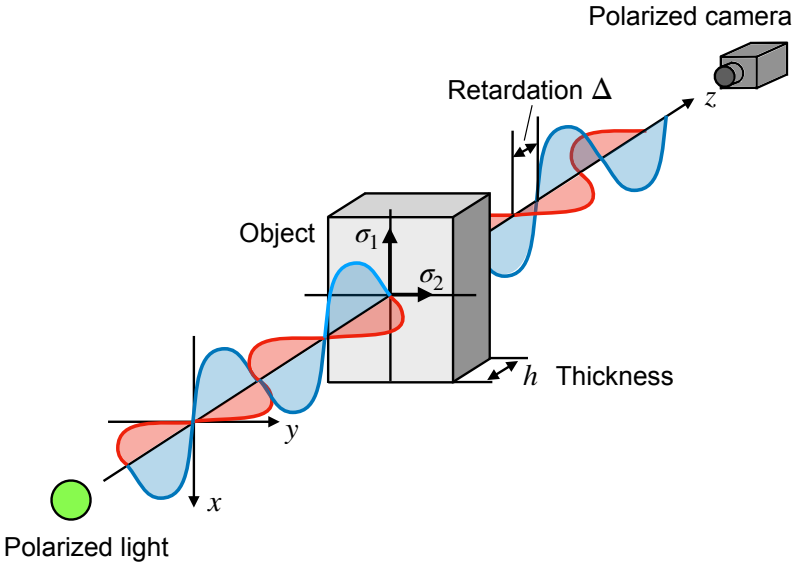

Figure 1. Illustration of a photoelastic method. σ_1 is the maximum principal stress in xy-plane, and σ_2 is the minimum principal stress. h is the thickness of measurement target. The light is a polarized light.

The purpose of this study is to elucidate the following two problems for CNC mixed solution (0.5 wt %). The first is to elucidate whether there are any phenomenon (trend) peculiar to CNC mixed solution that differ from those in the solid case. The second is to elucidate the extent to which the stress-optic law holds for CNC mixed solution. As a verification method for the first question, we conducted comparison and verification between the experimentally measured retardation distribution and the theoretical stress distribution based on the analytical solution in steady laminar flow in a rectangular channel for a CNC mixed solution (0.5 wt %) (Newtonian fluid). Also, as a verification method for the second question, we conducted comparison and verification between

the measured retardation, after offsetting the effect of the retardation peculiar to the CNC mixed solution us and the theoretical stress distribution.

2. Method

2.1. Experimental setup

Fig. 2 shows the schematic of our experimental set-up. It consists of a linear polarizer, a quarter-wave plate, and a rectangular channel (made of quartz) placed between a light source (SOLIS-525C, 525 nm, Thorlabs) and a high-speed polarization camera (CRYSTA P1-P, Photoron, imaging speed: 1,000 f.p.s.). The reason for using a rectangular channel is that the curvature of the channel surface, as in the case of a circular tube, refracts light and makes the difficulty of retardation measurement. The length of the channel is 60 mm and the size of the rectangular cross section is 2 mm $\times$ 2 mm. The high-speed polarization camera incorporates four polarizers with different polarization directions (0°, 45°, 90°, and 135°). The retardation of the incident light is calculated based on the light intensities of each polarizer (I_1, I_2, I_3, and I_4, respectively) (Onuma & Otani, 2014) as follows:

$$I_0 = \frac{I_1 + I_2 + I_3 + I_4}{2} \tag{2}$$

$$\Delta = \frac{\lambda}{2\pi} \sin^{-1} \frac{\sqrt{(I_3 - I_1)^2 + (I_2 - I_4)^2}}{I_0} \tag{3}$$

The working fluid is CNC (Alberta Pacific Co. Ltd.) mixed solution. CNC particles are tiny needle-like crystals that, when stressed, exhibit birefringence by orienting in the same direction to the stress (Frka-Petesic et al., 2015; Calabrese et al., 2021). CNC was mixed in ultra-pure water, stirred for more than one hour at 40°C using a stirrer (CHPS-170DF, ASONE Co., Ltd.) rotating at 600 rpm. The concentration of CNC solution was set to 0.5 wt %. Fig. 3 shows the results of shear viscosity measurement. Measurements were taken twice for the same concentration of fluid. The measured shear curve of the solution indicates that the solution can be regarded as a quasi-Newtonian fluid. In this paper, we approximated CNC mixed solution as Newtonian fluid. A syringe pump was used to flow the solution from a stationary state to a steady laminar flow. The maximum flow rate was set at 30 ml/min. To evaluate the validity, measurements were also conducted at different flow rates (10, 20 ml/min) (see section 3.4). The temporal evolution of retardation distribution was measured with the high-speed polarization camera. The flow direction is vertical to reduce the effect of particle precipitation. The coordinate system is set as shown in Fig. 2 where the position of the channel inlet is defined as x = 0 mm. The coordinate system is set as shown in Fig. 2 where the position of the channel inlet is defined as x = 0 mm. The measurement position was at x = 45 mm.

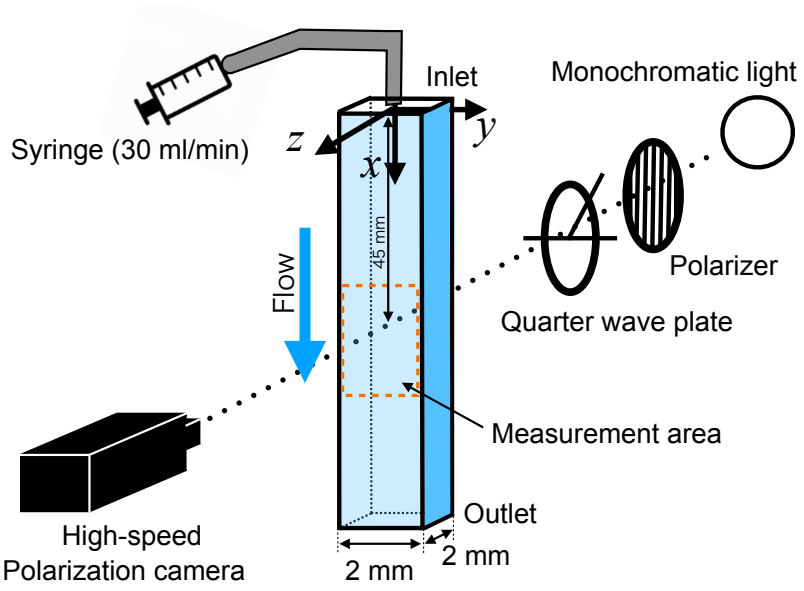

Figure 2. A schematic of the experimental set up.

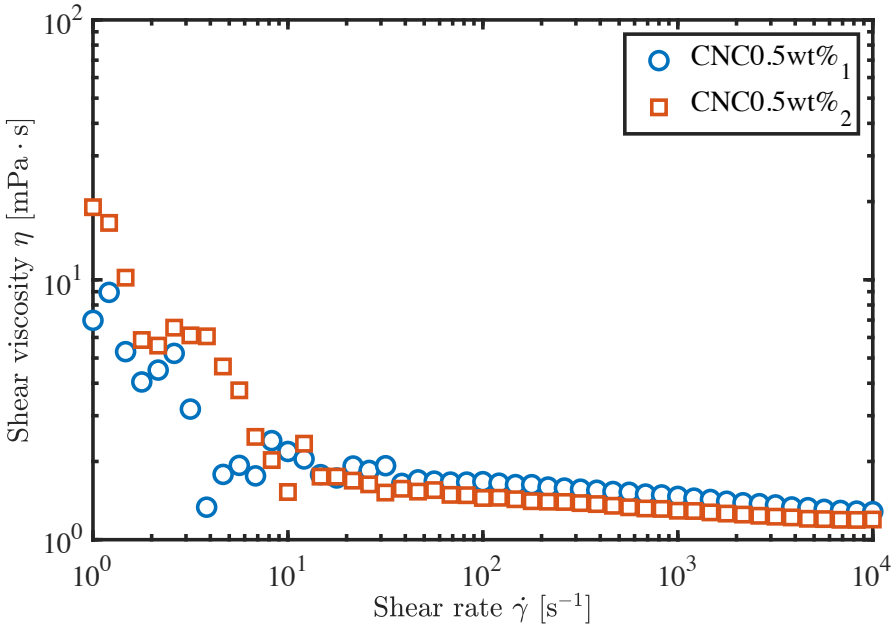

Figure 3. Shear viscosity μ versus shear rate $\dot{\gamma}$ in the cases of CNC mixed solution (0.5 wt %).

2.2. Theory

The velocity distribution u_x [m/s] of a steady laminar flow in a rectangular channel is derived Navier-Stokes equation (Delplace, 2018).

$$\left(\frac{\partial^2}{\partial y^2}+\frac{\partial^2}{\partial z^2}\right)u_x=-\frac{\Delta P}{\mu L} \tag{4}$$

where ΔP [Pa] is the pressure drop, μ [Pa·s] is the liquid viscosity, and L [m] is the channel length. From Eq. (4), the velocity distribution u_x is derived as

$$u_x(y,z)=\frac{16h^2\Delta P}{\pi^3\mu L}\sum_{n=0}^{\infty}\frac{(-1)^n}{(2n+1)^3}\left[1-\frac{\cosh\frac{(2n+1)\pi y}{2h}}{\cosh\frac{(2n+1)\pi w}{2h}}\right]\cos\frac{(2n+1)\,\pi z}{2h} \tag{5}$$

where w [m] is the channel width, and h [m] is the channel thickness. The calculated velocity distribution u is shown in Fig. 4.

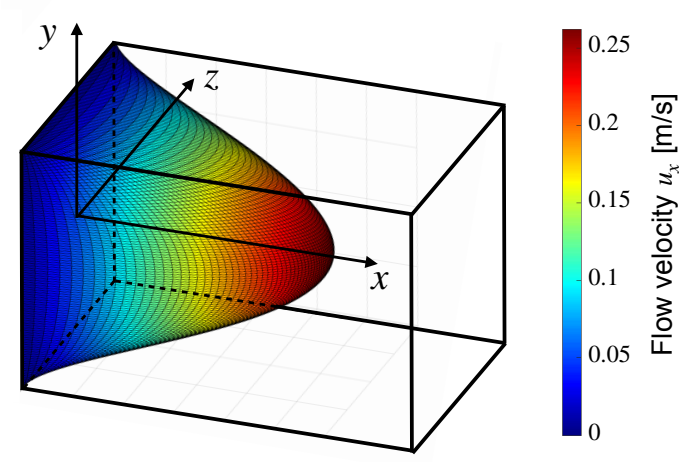

Figure 4. The theoretical velocity distribution in a rectangular channel (see Eq. (5)) with ΔP = 74.2 [Pa] and μ = 1.67 [mPa·s].

From the theoretical velocity distribution u_x shown in Eq. (5), we calculate the velocity gradient and stress tensor. From the calculated stress tensor, three principal stresses σ_{01}, σ_{02}, and σ_{03} ($\sigma_{01} > \sigma_{02} > \sigma_{03}$), which are orthogonal to each other, are obtained. The principal stress difference is then calculated from the difference between the maximum principal stress and the minimum principal stress . The principal stress difference distribution in the yz plane is shown in Fig. 5(a). Fig. 5(a) shows that the steady laminar flow in the rectangular channel has the three-dimensional stress distribution in z direction (the optical axis of the camera). The principal stress difference has the maximum value at the wall and the minimum value (0 Pa) at the center of the channel (y = 0 mm, z = 0 m). Here we must note that, in a three-dimensional stress field, the principal stress difference shown in Fig. 5(a) is unsuitable to be used as σ_d in Eq. (1). Instead, the "apparent" principal stress difference based on the secondary principal stress on the plane perpendicular to the optical axis of the camera (xy-plane) should be used (Doyle & Danyluk, 1978; Aben, 1982; Sampson, 1970). The apparent principal stress difference is given by the following equation;

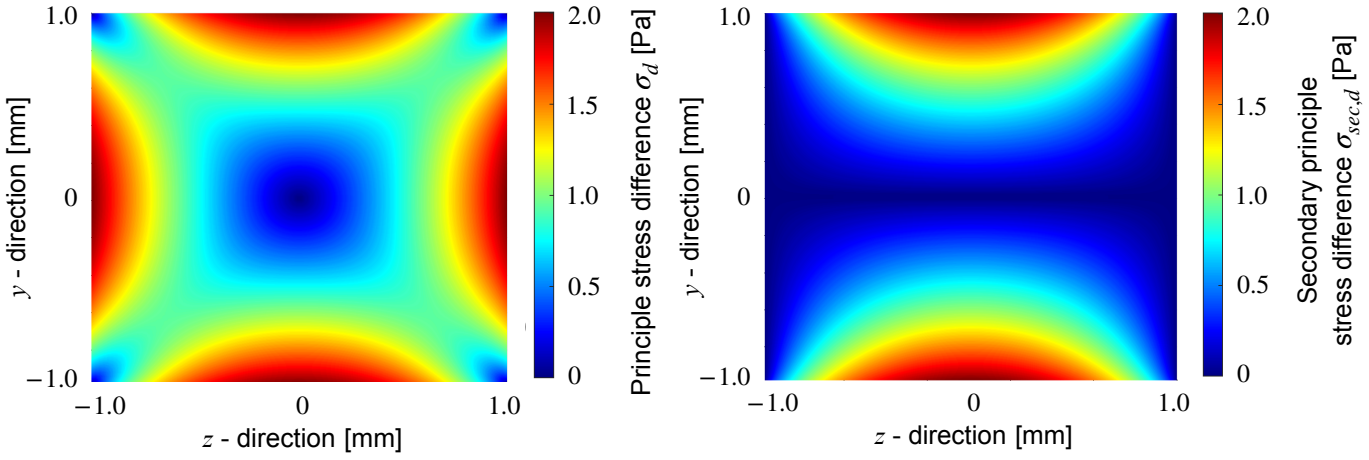

Figure 5. (a) The distribution of principal stress difference . (b) The distribution of secondary (apparent) principal stress difference.

$$\sigma_{sec,d} = \sqrt{(\sigma_{xx} - \sigma_{yy})^2 + 4\sigma_{xy}^2} \tag{6}$$

This $\sigma_{sec,d}$ is called the secondary principal stress difference. The secondary principal stress distribution in the measured cross section calculated using this equation is shown in Fig. 5(b). The value of the secondary principal stress difference near (y, z) = (0, $\pm$1) is smaller than that of the principal stress difference because the secondary principal stress difference ignores the shear stress due to the velocity gradient in z direction.

3. Result and discussion

3.1. Visualization results of retardation distribution and time variation of retardation

Fig. 6(a) shows the visualized image of the retardation distribution taken by the high-speed polarization camera. The time when the liquid started to flow was set to 0 ms, and the visualization images of the retardation distribution at each elapsed time are displayed. The value of the retardation increases with time. The retardation value was the smallest at the center of the channel (y = 0 mm) and largest at the wall (y = ±1 mm). The reason for this is that the velocity gradient, i.e. shear stress, near the wall is larger than that near the center of the channel. Fig. 6(b) shows temporal evolution of the mean retardation in the measurement area (orange dotted line in Fig. 2). The average retardation becomes almost constant after 1,800 ms, indicating that the flow becomes steady. Since the object of this paper is to clarify the relationship between the retardation and three-dimensional hydraulic stress field, we focus on a steady laminar flow in a rectangular channel.

3.2. Comparison results between theoretical and measured value

The measurement retardation Δ (Experimental value) and the calculated secondary principal stress difference $\sigma_{d,sec}$ (Theoretical value) are shown in Fig.7. As mentioned above, since the measurement result of the retardation is an integrated value along the optical axis of the camera (z-axis

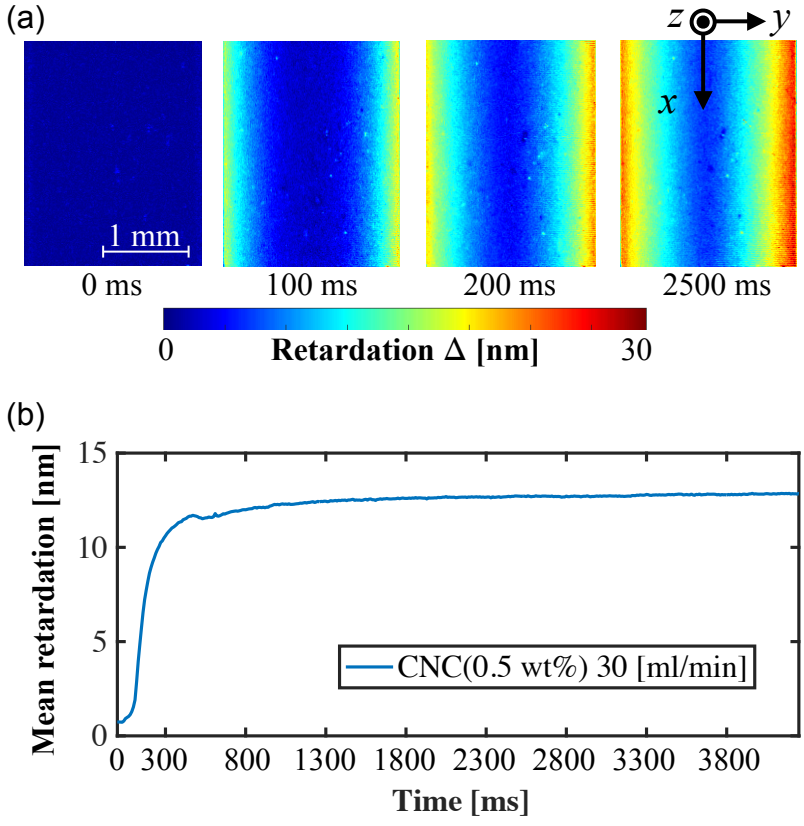

Figure 6. (a) Time transition of retardation measurement value of CNC (0.5 wt %) at flow rate of 30 ml/min. (b) Relaxation time of mean retardation of CNC (0.5 wt %) at flow rate of 30 ml/min.

direction), theoretical secondary principal stress difference was also integrated. The measured retardation was averaged over the spatial range (43 mm < x < 45 mm) and over the time period (2,800 ms to 3,800 ms) during which the flow was considered to be steady. Note that the area of analysis is outside the inlet region(x < 30 mm), and the flow is fully developed. From Fig. 7, both results have a maximum value at the channel wall (y = ± 1 mm), and a minimum value at the center of the channel (y = 0 mm). This indicated that there is a correlational relationship between the retardation Δ and the secondary principal stress difference $\sigma_{d,sec}$ int the stress field of the CNC mixed solution (0.5 wt %) as well. On the other hand, no proportional relationship is established between the two. In the stress-optic law, the stress-optic coefficient C is a material-specific physical property and a constant. Therefore, when the stress-optic law holds, the spatial intensity distributions of the retardation and the stress coincide. However, Fig. 7 shows that the error between the two distributions increases as one approaches the center of the channel (y = 0 mm). In the next section, we discuss the peculiar retardations that develop in the CNC mixed solutions.

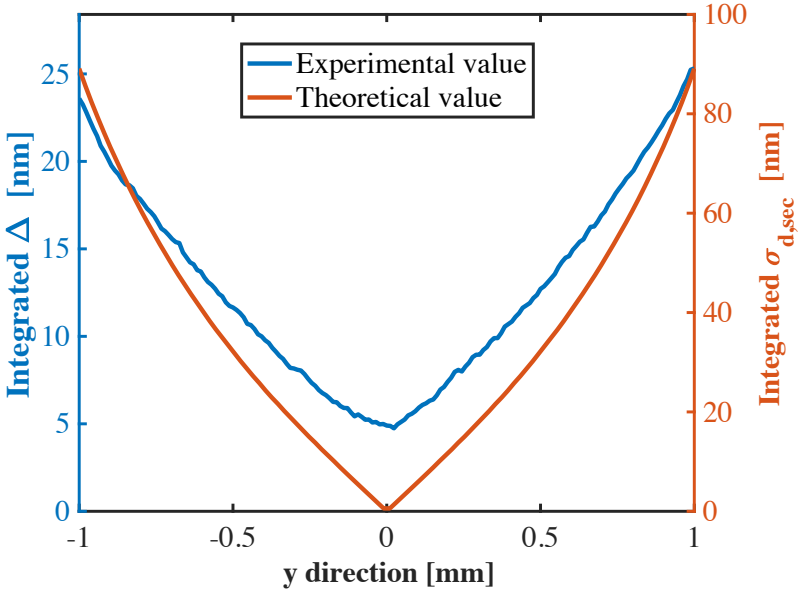

Figure 7. Comparison between distribution of secondary principal stress difference and measured retardation in y-direction of the CNC (0.5 wt %) solution at flow rate 30 ml/min.

3.3. Discussion about the retardation peculiar to this CNC mixed solution

We discuss the peculiar retardations that develop in the CNC mixed solutions in Fig. 7. One possible cause is the appearance of retardations due to aggregations of the CNC particles. CNC mixed solution is reported to develop retardations due to a factor unrelated to stress (Kádár et al., 2021). Specifically, as the shear rate applied to the CNC mixed solution increases, the CNC particles aggregate with each other. As a result, a spatial anisotropy arises and a retardation that is not due to stress develops. This was also confirmed by retardation measurements conducted in our laboratory. We measured the CNC mixed solution under simple shear flow by using a rheometer (MCR302, Anton Paar Co., Ltd.) and a high speed polarization camera. Fig. 8 shows the schematic of experimental setup (a, b) and results (c). The gap height between quarter wave plate and transparent stage is fixed at 0.10 mm. The shear rates $\dot{\gamma}$ applied to the working fluid are

1,000, 5,000, 10,000 s^{-1} . When the simple shear flow induced by the rheometer is viewed along the z-axis, the secondary principal stress difference $\sigma_{d,sec}$ is zero. Therefore, no retardation is expected to appear. In fact, however, a retardation corresponding to the shear rate of the rotating plate was measured (Fig. 8(c)). The proportional relationship between the retardation and shear rate is obtained as

$$\Delta_{st} = C_{st} dh\dot{\gamma}, \tag{7}$$

where Δ_{st} is aggregation-induced retardation. C_{st} is a proportional coefficient calculated from the result (Fig. 8(c)). and the value is 8.0×10^{-8} s. dh is the gap height and the value is 0.1 mm. This phenomenon is unique to the CNC mixed solution. Therefore, in the CNC mixed solution, not only stress-induced retardations but also aggregation-induced retardation is observed.

Based on the above, in the next section, we will compare the theoretical value with the retardation that offsets the effect of retardations specific to the CNC mixed solution. Then we discuss the range of applicability of the stress-optic law to the CNC mixed solution.

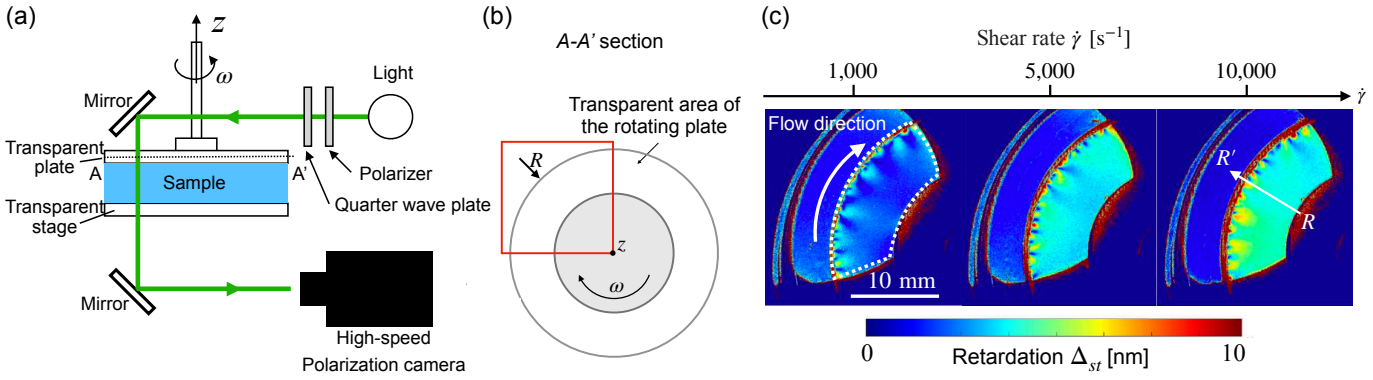

Figure 8. (a) A schematic of the experimental setup of measuring retardation distribution by using a rheometer. The measurement area is surrounded by red line in (b) A-A' section. (c) spatio-temporal average of phase retardation of CNC mixed solution (0.5 wt %) versus shear rate $\dot{\gamma}$ (= 1,000, 5,000, and 10,000 s^{-1})

3.4. Comparison results of retardation (offset) and second-order principal stress difference

Fig. 9 shows the result of a comparison between the measured retardation, after offsetting the effect of the retardation peculiar to the CNC mixed solution using Eq. (7)(Experimental value (offset)), and the the secondary principal stress difference (Theoretical value). This result indicates that the retardation, which eliminates the effect of the retardation specific to the CNC mixed solution, agrees with the theoretical value derived from the stress-optic law with a relative error of 3.84 %.

To evaluate the validity of the above validation results, conducted the same verification and tested the results in different stress fields As a method of varying the stress field, we conducted at different flow rates (10, 20 ml/min). The results are shown in Fig. 10. Fig. 10(a, b) show the calculated secondary principal stress difference and measured retardation at flow rates of 10 ml/min and 20 ml/min, respectively. The results show that both values increase with an increase in flow velocity. Fig. 10(c, d) show the spatial intensity distribution of the secondary principal stress difference (Theoretical value) and the spatial intensity distribution of retardation offsetting the effect of the retardation specific to the CNC mixed solution (Experimental value (offset)) at flow rates of 10

ml/min and 20 ml/min, respectively. For a flow rate of 10 ml/min, both distribution agree with a relative error of 5.67 %. And for a flow rate of 20 ml/min, both distribution agree with a relative error of 3.24 %. These results indicate that the validation results are valid for different flow rates (different stress fields).

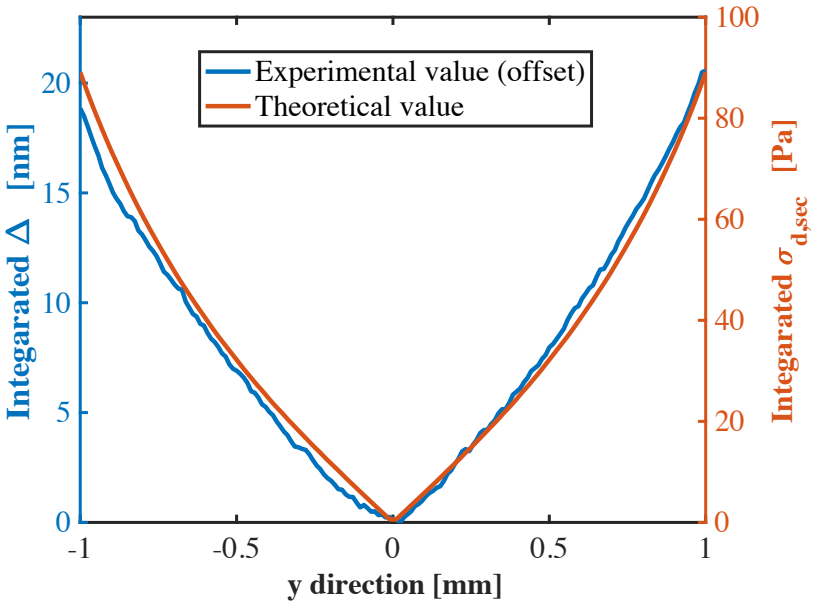

Figure 9. Comparison between distribution of secondary principal stress difference and retardation (offsetting the effect of the retardation peculiar to CNC mixed solution) of the CNC (0.5 wt %) solution at flow rate 30 ml/min.

4. Conclusion

In this study, we measured retardation of steady laminar flow in a rectangular channel for the CNC mixed solution (0.5 wt %) (Newtonian fluid). As a result, We success in taking visualized image of retardation distribution. Based on the results, we investigated whether there are any phenomena (trends) peculiar to the CNC mixed solution that differ from those in the solid case. We conducted comparison and verification between the experimentally measured retardation distribution and the theoretical secondary principal stress difference distribution based on the analytical solution in steady laminar flow in a rectangular channel. We compare the distributions of the experimentally measured retardation and the theoretical secondary principal stress difference. The result showed that a retardation, which was not caused by stress, appeared in the CNC mixed solution. The cause is considered to be the retardation caused by the aggregations of the CNC particles. This phenomenon does not occur in solids cases. In addition, We investigated the extent to which the stress-optic law holds for the CNC mixed solution. The result showed that the spatial intensity distributions of both agreed within a relative error of 3.84 %. This indicates that the stress-optic law holds for the retardation offsetting the retardation specific to the CNC mixed solution. To evaluate the validity of the above validation results, we conducted experiments with different flow rates (10, 20 ml/min). As a result the relative errors from theoretical values were 5.67 % and 3.24 % for flow rates of 10 and 20 ml/min, respectively. These results indicate that the method presented here is promising for measuring three-dimensional stress field in a flow.

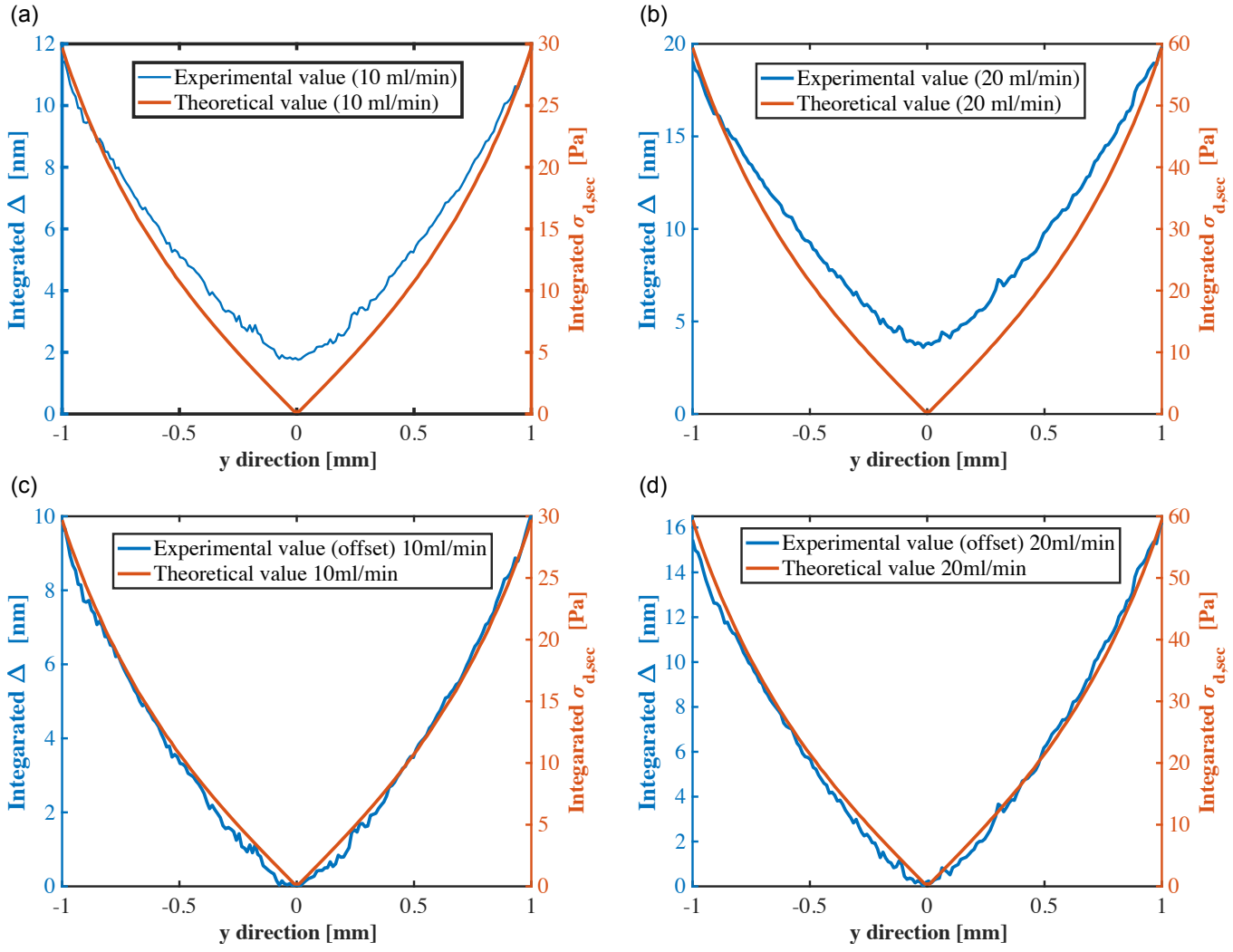

Figure 10. (a), (b) show the calculated secondary principal stress difference and measured retardation at flow rates of 10 ml/min and 20 ml/min, respectively. (c), (d) show the secondary principal stress difference (Theoretical value) and the retardation offsetting the effect of the retardation specific to the CNC mixed solution (Experimental value (offset)) at flow rates of 10 ml/min and 20 ml/min, respectively.

5. Acknowledgment

This work was funded by Japan Society for the Promotion of Science (Grant No. 20H00223, 20H00222, and 20K20972) and Japan Science and Technology Agency PRESTO (Grant No. JPMJPR21O5).

References

Aben, H. (1982). Integrated photoelasticity of axisymmetric bodies. *Optical Engineering*, *21*(4), 689–695.

Calabrese, V., Haward, S. J., & Shen, A. Q. (2021). Effects of shearing and extensional flows on the alignment of colloidal rods. *Macromolecules*, *54*(9), 4176–4185.

Delplace, F. (2018). Laminar flow of newtonian liquids in ducts of rectangular cross-section a model for both physics and mathematics. *Open Access J. Math. Theor. Phys.*, *1*, 198–201.

Doyle, J. F., & Danyluk, H. (1978). Integrated photoelasticity for axisymmetric problems. *Experimental Mechanics*, *18*(6), 215–220.

Frka-Petesic, B., Sugiyama, J., Kimura, S., Chanzy, H., & Maret, G. (2015). Negative diamagnetic anisotropy and birefringence of cellulose nanocrystals. *Macromolecules*, *48*(24), 8844–8857.

Kádár, R., Spirk, S., & Nypelo, T. (2021). Cellulose nanocrystal liquid crystal phases: Progress and challenges in characterization using rheology coupled to optics, scattering, and spectroscopy. *ACS nano*, *15*(5), 7931–7945.

Meng, H., Wang, Z., Hoi, Y., Gao, L., Metaxa, E., Swartz, D. D., & Kolega, J. (2007). Complex hemodynamics at the apex of an arterial bifurcation induces vascular remodeling resembling cerebral aneurysm initiation. *Stroke*, *38*(6), 1924–1931.

MUTO, M., & TAGAWA, Y. (2019). Development of experimental visualization method for hydrodynamic stress field. , *38*(6), 419–422.

Onuma, T., & Otani, Y. (2014). A development of two-dimensional birefringence distribution measurement system with a sampling rate of 1.3 mhz. *Optics communications*, *315*, 69–73.

Ramesh, K. (2021). *Developments in photoelasticity*. IOP Publishing.

Sampson, R. C. (1970). A stress-optic law for photoelastic analysis of orthotropic composites. *Experimental Mechanics*, *10*(5), 210–215.

Shojima, M., Oshima, M., Takagi, K., Torii, R., Hayakawa, M., Katada, K., … Kirino, T. (2004). Magnitude and role of wall shear stress on cerebral aneurysm: computational fluid dynamic study of 20 middle cerebral artery aneurysms. *Stroke*, *35*(11), 2500–2505.